MAY 1983 LRP 222/83

GEOMETRICAL EFFECTS ON THE ABSORPTION OF MHD WAVES AT THE ALFVEN SPATIAL RESONANCE

S. Succi, K. Appert, A.H. Kritz and J. Vaclavik

GEOMETRICAL EFFECTS ON THE ABSORPTION OF MHD WAVES AT THE ALFVEN SPATIAL RESONANCE

S. Succi, K. Appert, A.H. Kritz* and J. Vaclavik

Centre de recherches en Physique des Plasmas
Association Euratom - Confédération Suisse
Ecole polytechnique Fédérale de Lausanne
CH-1007 Lausanne - Switzerland

* Permanent address: Dept. of Physics, Hunter College, CUNY

ABSTRACT

Recent advances of MHD theory of Alfvén Wave Heating have shown evidence of several novel features. These features are related to the inclusion of the Hall term and to the inclusion of shear and curvature of the magnetic field lines in cylindrical plasmas. It is important to ascertain the extent to which these features are retained in a simpler geometry such as a slab. We have employed a cold, current-carrying plasma model for a slab of finite thickness, in order to compare results with those already obtained using other models. We show that some phenomena have similar behaviour in a slab plasma as in a cylindrical plasma. However, the general conclusion is that the slab geometry provides a qualitatively correct model for only some of the features relevant to Alfvén Wave Heating.

1. INTRODUCTION

It has been shown that the effects associated with a finite ion-cyclotron frequency can significantly influence the MHD description of resonant absorption of magnetoacoustic modes at the Alfvén spatial resonance. For example, CRAMER and DONNELLY (1982) have carried out analytic studies for a plane semi-infinite plasma illustrating the effects of finite ion-cyclotron frequency. These effects have also been demonstrated numerically in cylindrical geometry by APPERT and VACLAVIK (1983). Moreover, it has been shown that the magnetic field curvature and shear (APPERT et al., 1982 a) can play a non-negligible role in the context of absorption. In order to obtain a tokamak modelling for the Alfvén wave heating scheme, it is desirable to determine which physical features can be retained in a simple geometry, namely a slab of finite thickness. A simple geometry would allow for the inclusion of a more complete physical description of the plasma behaviour. Therefore, a cold, current-carrying, plasma slab model is used, and the results obtained are compared with the results obtained using a cylindrical model.

In order to simulate field line curvature, we introduce a gravitational field, acting in a direction perpendicular to the main magnetic field component. From the equilibrium equations, it follows that the gravity field provides an additional centrifugal force on the plasma motion. We include the effect of the Hall term in the same way it was included by APPERT and VACLAVIK (1983).

The paper is structured as follows: In Section 2, we write down the basic equations of our model, and in Section 3, we discuss the spectral properties for the homogeneous currentless plasma. We present typical results for resonant absorption in Section 4. Section 5 contains a discussion of the global eigenmodes of the Alfvén Wave. Finally, in Section 6, we present the main conclusions.

2. BASIC EQUATIONS

We are concerned with small amplitude perturbations that have frequencies much less than lower hybrid frequency. The plasma we consider is a cold, current-carrying plasma slab of finite thickness. Linearization of the equation of motion and Ohm's law leads to the following equations:

$$\rho_0 \partial \vec{v}/\partial t = \frac{1}{c}\left(\vec{j}_0 \times \vec{B} + \vec{j} \times \vec{B}_0 \right) + \rho \vec{g} \qquad (1)$$

$$\vec{E} + \vec{v} \times \vec{B}_0/c = (m_i/ec\rho_0)\left(\vec{j}_0 \times \vec{B} + \vec{j} \times \vec{B}_0 \right) \qquad (2)$$

Here $\vec{v}$ denotes the plasma velocity; $\vec{j}$ the current; $\vec{E}$, $\vec{B}$, and $\vec{g}$ the electric, magnetic and gravitational fields, respectively; ρ the mass density; c the speed of light, m_i the ion mass; and e the electron charge. Equilibrium quantities are labelled with the subscript 'o'.

We assume a one-dimensional layer model, so that all the equilibrium quantities depend only on the x space coordinate (radial), with no variation along the y (poloidal) and z (toroidal) directions. Consequently, we introduce the usual "ansatz" $e^{i(kz+my-(\omega+i\nu)t)}$ for the perturbed quantities, with k representing the "toroidal" and m, the "poloidal" wavenumber. We shall consider the limit $\nu \longrightarrow 0^+$.

Equations (1) and (2), together with Maxwell's equations and the mass continuity equation, yield a wave equation for the electric field vector. With use of $E_\perp$ and $B_\parallel$ as the unknows, the wave equation can be cast in the elegant form given below :

$$A\, dE_\perp/dx = G k_\perp E_\perp + i\omega \left(A - k_\perp^2 \right) B_\parallel \qquad (3a)$$

$$A\, dB_\parallel/dx = (i\omega)^{-1} \left(G^2 + AD \right) E_\perp - G k_\perp B_\parallel \qquad (3b)$$

with

$$A = \omega^2 (1-\xi^2)^{-1} - k_\parallel^2 \qquad G = \omega^2 \xi (1-\xi^2)^{-1} \qquad D = \frac{g\, d\rho_o/dx}{B_o^2} - A \qquad (4)$$

where $\xi = \omega/\omega_{ci}$. All variables in Eqs. (3a) and (3b) are normalized using the standard MHD scaling. Length is expressed in units of the slab half-width, a, and the time, in units of Alfvén transit time $a/c_A(0)$ where $c_A(0)$ is the Alfvén wave speed at x = 0, the mid-plane of the plasma slab. The magnetic field is in units of $B_{0z0} = B_{0z}(0)$ and the electric field in units of $c_A(0) B_{0z0}/c$. Plasma density is scaled by its value on the plasma mid-plane.

A local coordinate system is defined throughout the plasma by:

$$\hat{e}_{\parallel} = \vec{B}_0 / B_0 \qquad \hat{e}_{\perp} = \hat{e}_{\parallel} \times \hat{x}$$

where the caret indicates unit vectors. The parallel and perpendicular wavevector components are then written:

$$k_{\parallel} = (k B_{0z} + m B_{0y}) / B_0 \qquad k_{\perp} = (m B_{0z} - k B_{0y}) / B_0$$

We point out that m must be regarded as a step function, that is, $m(x) = m \cdot \mathrm{sgn}\,(x)$. This artificial definition is neeeded to guarantee the correct symmetry with respect to the x coordinate. Finally, we assume that beyond the plasma there is a vacuum region and then a perfectly conducting plane. The conducting plane is located at $x = \pm x_S$, where $x_S > 1$ (the normalized slab half-width). In general, if f(x) designates any discontinuous antisymmetric function, the notation f will stand for its right-hand side value.

As in APPERT and VACLAVIK (1983), we assume that plasma oscillations are excited by an idealized antenna, consisting of a sheet current with a given frequency, ω, and helicity, k/m. This antenna is situated symmetrically on planes located at $x = \pm x_A$. In dimensionless units, the antenna current is:

The boundary value problem is fully specified by imposing electric and magnetic field continuity at the plasma edge together with vanishing electric field at the conducting shell and by imposing the appropriate jump condition at the antenna.

Equations (3a) and (3b) are solved numerically for the plasma region. We match this solution to the vacuum solution which is obtained analytically. Once the full solution is found, we calculate the power absorbed per unit area in the plasma. This is given by

$$p = - \lim_{\varepsilon \to 0} < \int_{x_A - \varepsilon}^{x_A + \varepsilon} (\vec{\gamma} \cdot \vec{E}^*) \, dx >$$

where brackets denote time averaging over a wave period. Solutions of the boundary value problem, specified above, are sought for a range of values of the available free parameters. Particularly we consider the frequencies ω and ω_{ci} and the wavenumbers k and m. We specify "standard conditions" with the following equilibrium profiles:

$$\rho_0(x) = 1 - 0.95|x| \qquad B_{0z}(x) = 1 \qquad \gamma_{0z}(x) = 0.6\,(1-x^2)^2$$

and the choice,

$$x_A = 1.2 \qquad x_S = 1.5$$

Since the situations we investigate exhibit spatial symmetry with respect to the x coordinate, we shall confine our study to the right half-side of the plasma slab, i.e., $0 \leq x \leq 1$.

3. HOMOGENEOUS CURRENTLESS PLASMA SLAB

We consider a homogeneous currentless plasma, without the gravity field. For this plasma in equilibrium, Eqs (3a) and (3b) are amenable to an analytical treatment. Assuming that the perturbed fields vary as $\exp(k_x \cdot x)$, we obtain the following solution:

$$E_\perp = C \cdot F_s(k_x x) \tag{5}$$

$$B_\parallel = C \cdot \left(\frac{m(x)\, G/A}{m^2 - A} \cdot F_s(k_x x) + \frac{k_x A}{m^2 - A} F_c(k_x x) \right) \tag{6}$$

where k_x, the wavevector component in the x direction, is given by

$$k_x^2 = m^2 - A + G^2/A \tag{7}$$

and C is an arbitrary multiplicative constant. The symbols F_s and F_c denote either hyperbolic or trigonometric sine and cosine functions, depending on whether k_x^2 is greater or less than zero. The presence of the odd function in the expression for $B_\parallel$, Eq. (6), is surprising at first glance. However, it is due to the discontinuity of the factor $(G/A)\, m(x)/(m^2-A)$, resulting from the definition of $m(x)$.

Imposing the boundary conditions, one finds:

$$k_x \operatorname{cth}(k_x) = m\, G/A + (m^2 - A) \operatorname{cth}\left(\mu |x_s - 1|\right) \tag{8}$$

where $\mu = (k^2 + m^2)^{1/2}$. The combination of Eqs. (7) and (8) leads to the exact finite slab dispersion relation. We remark that in the limit of large values of k_x and x_s, Eq. (8) reduces to

$$k_z = mG/A + k^2(m^2 - A)/A\mu \quad , \quad k_x^2 > 0$$

This coincides with the expression reported in CRAMER and DONNELLY (1982) the semi-infinite slab, occupying the half-space $x < 0$.

The presence of $\mathrm{cth}(k_x)$ and $\mathrm{cth}[\mu\,|\,x_s - 1\,|\,]$ in Eq. (8) is a consequence of the finite size of the system. The combination of Eqs. (7) and (8) yields a trascendental equation which could be solved with standard numerical techniques. The utility of this procedure is limited to the homogeneous currentless plasma. Since we intend to discuss more general situations, we follow the numerical approach outlined in Section 2. We consider excitation of the plasma due to an external antenna and numerically calculate the antenna load as a function of the applied frequency. Any peak that appears in the antenna load indicates the presence of an eigenmode.

First Radial Mode ("Surface Mode")

It has been recently recognized (CRAMER and DONNELLY, 1982; APPERT and VACLAVIK, 1983) that the Hall term splits the first radial mode (F_1) of the fast magnetosonic wave into two branches, $F_1(m > 0)$ and $F_1(m < 0)$. The dispersion relation of these branches appears quite different when the wave field helicity $k/m \simeq 1$. In a plane semi-infinite plasma, the $F_1(m < 0)$ mode always has surface character,

i.e. $k_x > 0$. For the other mode $F_1 (m > 0)$, k_x can become negative for k/m greater than a certain value, (CRAMER and DONNELLY, 1982). This implies that beyond this value, the mode looses its surface character. In addition, it also looses physical meaning because the amplitude becomes unbounded at infinity. In our case, since we consider a slab of finite thickness, this argument does not hold, and both signs of k_x must be retained. The nature of the mode in our analysis is not determined by the sign of k_x. Nonetheless, we shall use the terminology "surface" mode to denote the $F_1 (m < 0)$ mode.

Our computational results for a plasma slab of finite thickness have shown good agreement with the previous results (CRAMER and DONNELLY, 1982; APPERT et al., 1983) in the range $0 < k/|m| < 0.7$ (Figs. 1a, 1b). As the ratio $k/|m|$ is increased to 1 and greater, the frequencies of the $F_1 (m > 0)$ mode deviate from the values obtained for the plane semi-infinite plasma and the cylindrical plasma. However, for the "surface" mode, the dependence of frequency on k is in good agreement with the results obtained both for the plane semi-infinite plasma and for the cylindrical plasma. These computational results can be qualitatively explained as follows: As previously mentioned, for the mode $F_1 (m > 0)$ mode in the plane semi-infinite plasma, k_x decreases and tends to assume negative values as $k/|m|$ increases. In the slab of finite thickness, when k_x tends to zero, the left-hand side of Eq. (8) still maintains a value greater than one. This is due to the presence of the factor $\mathrm{cth}(k_x)$, which reflects the finiteness of the geometry. Therefore, to satisfy Eq. (8), a wave frequency rearrangement is needed in order to produce the corresponding increase on the right hand-side. This increase can be effectively achieved by letting the coefficient A tend to zero, which corresponds to the mode

frequency tending towards the Alfvén wave frequency. The same argument does not apply to the $m < 0$ mode, whose frequency is already brought close to the Alfvén wave frequency by the Hall term.

Higher Radial Modes (cavity modes)

The Hall term together with the finiteness of the slab remove the degeneracy of the fast modes with respect to the m wavenumber in the small k region. This leads to distinct cut-off frequencies. Analysis of Eqs. (7) and (8) in the limit $k \to 0$ yields:

$$k_x^2 \sim m^2 - \omega^2 \tag{9}$$

$$k_x \, \mathrm{eth}(k_x) \sim m\,\omega/\omega_{ci} \tag{10}$$

In the plane semi-infinite plasma, the factor $\mathrm{cth}(k_x)$ does not appear in Eq. (10). In this case k_x is antisymmetric with respect to m. Therefore, using Eq. (9) one finds:

$$\omega_{\text{cut-off}}^{(-m)} = \omega_{\text{cut-off}}^{(+m)} = |m| \Big/ \left(1 + m^2/\omega_{ci}^2\right)^{1/2}$$

However, in the slab of finite thickness, the presence of the $\mathrm{cth}k_x$ factor breaks the k_x antisymmetry with respect to m. As a result, there are two distinct cut-off frequencies, i.e., one for each sign of m. This is shown in Fig. 1a and 1b. Equations (9) and (10) can be used to show that for a slab of finite thickness the cut-off frequencies have the property

$$\omega_{\text{cut-off}}^{(m<0)} > \omega_{\text{cut-off}}^{(m>0)}$$

It is interesting to point out that in the finite slab, this property does not depend on the distance between the conducting wall and the plasma boundary. This is a consequence of the fact that the k^2 factor in Eq. (8) always dominates over the cth $[\mu|x_s - 1|]$ factor. Thus, even in the limit $x_s = 1$, the second term on the right-hand side of Eq. (8) vanishes for $k \to 0$. In contrast, for a cylindrical plasma (APPERT et al., 1983) the cut-off frequencies do not change with the sign of m unless $x_s \simeq 1$. Therefore, in the cylindrical case, there are two distinct cut-off frequencies only when $x_s \simeq 1$.

4. DIFFUSE EQUILIBRIUM PROFILES

For the inhomogeneous plasma, the most relevant feature is the appearance of a continuum in addition to the usual discrete spectrum. This continuum corresponds to the condition A = 0 in Eq. (4). This yields:

$$\omega_A = |k_{\parallel} c_A| \Big/ \left(1 + k_{\parallel}^2 c_A^2 / \omega_{ci}^2\right)^{1/2} \tag{11}$$

where

$$k_{\parallel} c_A = \left(k + m B_{oy}\right) \Big/ \rho_0^{1/2} \tag{12}$$

From Eqs. (11) and (12) we note that the dependence of ω_A on x arises both from the plasma inhomogeneity, $\rho_0(x)$, and from the

current, which is responsible for the sheared magnetic field structure $B_{oy}(x)$. A general analytical treatment is not feasible if the plasma equilibrium is not homogeneous. Therefore, we find it necessary to utilize a numerical description to investigate the effects of shear, curvature and the Hall term, i.e., ω/ω_{ci}.

A peculiar property of the slab geometry is that shear monotonically increases from the center of the plasma to the boundary, in accordance with Ampere's law:

$$B_{oy}(x) = \int_0^x j_{oz}(x')\,dx'$$

As a consequence, a monotonic $\omega_A(x)$ profile can never be achieved when k and m are of the opposite sign if a parabolic density profile is assumed. A monotonic $\omega_A(x)$ profile can instead be obtained with a linear density profile (see standard conditions, defined in Section 2). A second consequence is that the plasma has enhanced capability for resonantly absorbing energy at the periphery, even in the limit of vanishing k. Therefore, there is a monotonic decrease of optimal power (defined below) as a function of k. (See Fig. 2) This result is different from the one obtained for the cylindrical plasma. The optimal power $p^{opt}(k)$ is defined as Max $[p(x_R,k)\}$ for $0 \leq x_R \leq 1$, where $p(x_R,k)$ designates the power resonantly absorbed when the resonant layer is located at x_R and the wave number equal k. The optimal resonant layer position $x_R^{opt}(k)$, is the value of x_R where $p^{opt}(k)$ is attained. As in the cylindrical case (APPERT and VACLAVIK, 1983), when shear is removed, the power absorption is forced to zero since ω_A tends to zero when $k \longrightarrow 0$. Consequently, p^{opt} has a maximum for non-zero k. From Figs. 2a and 2b, we realize that

the optimal power is higher in the shearless case (except for small values of k). On the other hand, when shear is present, the power is more readily deposited near the center of the plasma.

This result is similar to the one obtained for the cylindrical geometry.

We next consider the effect of the curvature of the field lines. It has been shown by APPERT et al. (1982 a) that the curvature can influence power absorption in cylindrical plasmas by shifting the position of the optimal resonance layer to the innermost regions. In slab geometry, we simulate curvature by means of an external gravitational field. Consistent with equilibrium requirements, the gravity field is given by

$$\vec{g} = (\beta_{oz} B_{oy}/\rho_o)\,\hat{x}$$

Computational results, under standard condition defined in Section 2, indicate that g can simulate the effect of curvature only for very small values of k (Fig. 3). For small k the inclusion of g leads to a small increase in energy deposition near the center. However, as we shall see below, the gravity field can produce global eigenmodes of the Alfvén wave.

In previous work that focussed on the Hall term (APPERT and VACLAVIK, 1983) it has been shown that the position of the optimal resonant layer can be controlled via the ω/ω_{ci} parameter. For some

special choices of the wavenumber k, with m equal to plus or minus one, the shift of resonant layer position, is also accompanied by a relevant increase in the amount of power absorbed. In the finite-slab case, this control capability seems to be much less efficient for positive k and m (Fig. 4a, 4b and 5b). Instead, we observe a decrease in $p(x_R)$ for a given k, and the location of the optimal resonant layer position seems to be rather insensitive to variations of ω/ω_{ci}. For k and m both negative, the amount of absorbed power is strongly enhanced as in cylindrical geometry. However, the position of optimal resonant layer is shifted towards the edge of the plasma (see Fig. 5a). This result is surprisingly different from the result obtained for the cylindrical plasma with m = 1. On the other hand, we find that for the cylinder with m = 2, there is not a clear shift of the resonant layer position due to variation of ω/ω_{ci}. We conclude that m = 1 is a very special case for the cylinder. When m = 1, one wavelength encircles the whole cylinder. There is not a corresponding situation for the plasma slab.

5. GLOBAL EIGENMODES OF THE ALFVEN WAVE (GEAW)

In a cylindrical plasma and within the framework of ideal MHD description, the global eigenmodes are a result of curvature of the magnetic field lines (APPERT et al., 1982 b). In the present Section we show that a gravitational field can also produce these modes in a finite plasma slab configuration. The frequencies of these modes are expected to lie just below the lower edge frequency, ω_{LE}, of the continuum. The frequency, ω_{LE}, is obtained as a function of k by

minimizing the Alfvén frequency $\omega_A = (k+mB_{0y})/\rho_0^{1/2}$ with respect to the x variable. For the m = + 1 case, we distinguish three regions:

I) $k < -B_y(1)$

The lower edge frequency $\omega_{LE}(k)$, is implicitely defined as: $\omega_{LE} = \omega_A(k, x_{MIN}(k))$ where x_{MIN} satisfies the condition $\partial\omega_A/\partial x = 0$. In the spectral plane, i.e., the (k, ω) plane, $\omega_{LE}(k)$ is represented by a smooth line that starts from the point (-By(1), 0) and asymptotically approaches the ω = -k line. (See Fig. 6).

II) $-B_y(1) \leq k < 0$

In this region, $\omega_{LE} = 0$ since there is always a value of x in the range [0, 1] such that $B_y(x) + k = 0$.

III) $k \geq 0$

Since B_y is a monotonically increasing function of x, we obtain $\omega_{LE} = k$, which corresponds to the resonant layer always located at x = 0.

Region I

Numerical results with m = +1 under standard MHD conditions ($\omega_{ci} \infty$), show global modes in a fairly narrow range of k. Global eigenmodes emerge from the continuum at $k \gtrsim -0.5$. These modes rapidly become unstable, i.e., $\omega^2 < 0$, so that they disappear for $k \lesssim -0.37$.

Region II

In region II no stable mode can exist, since the continuum reaches marginal points ($\omega = 0$) for any k.

Region III

A local expansion of Eqs. (3a) and (3b) around $x = 0$ provides the following existence condition: $[(dD/dx)/(dA/dx)] > 0$, with D and A defined in Section 2. In principle, this condition can be fulfilled with standard profiles (described in Section 2). However, no numerical evidence of this has been produced. Consequently, we introduced an inconsistent gravitational field of the form $g(x) = g\ \mathrm{sgn}(x)$. This artificial gravity is efficient in producing the global modes of the Alfvén Wave for a range of k values. The location of this range is controlled by g, the magnitude of the "curvature". A constant gravity in the half-plane is certainly somewhat artificial, but, nevertheless recalls the fact that in a cylindrical plasma the ratio $B\theta/B_z$ is not zero (but generally maximum) on the axis. Numerical studies with parabolic density profiles suggest that $g > 0$ on the axis is (at least numerically) responsible for the occurrence of GEAW in the $k > 0$ range.

CONCLUSIONS

We have investigated some properties of the low-frequency spectrum of cold plasma waves. Comparisons with cylindrical and plane semi-infinite models have been systematically carried out, in an attempt to identify those properties whose occurrence is independent of the geometry. We have shown that the radial modes of the fast magnetosonic wave can be partially influenced by slab finiteness and by the Hall term, or by both combined. Fortunately, the "surface" wave which is the best candidate for the Alfvén Heating scheme, behaves rather insensitively to geometrical details.

We have found that: 1) When frequencies in the continuum are excited, the gravitational field can simulate cylindrical curvature only for small "toroidal" wavenumbers. 2) The gravitational field can produce global eigenmodes of the Alfvén wave. 3) Shear enhances power absorption in the near plasma center, but generally reduces the amount of absorption. 4) For $k > 0$ and $m = +1$, the Hall current influences the location of the optimal resonant layer less in the case of the finite plasma slab than in the case of the cylindrical plasma.

In general, we conclude that only some of the primary physical features of Alfvén Wave Heating can be recovered in the slab geometry.

REFERENCES

[1] APPERT K., BALET B. and VACLAVIK J. (1982 a), Phys. Lett. 87A, 233.

[2] APPERT K., GRUBER R., TROYON F. and VACLAVIK J. (1982 b), Plasma Physics 24, 1147.

[3] APPERT K. and VACLAVIK J. (1983) Plasma Physics, 25, 551.

[4] APPERT K., VACLAVIK J. and VILLARD L. (1983), Spectrum of Low-Frequency, Non Axisymmetric Oscillations in a Cold Current-Carrying Plasma Column, Lausanne Report LRP 218/83, submitted for publication to Phys. Fluids.

[5] CRAMER N.F. and DONNELLY I.J. (1982), Fast and Ion Cyclotron Surface Waves at a Plasma-Vacuum Interface, submitted to Plasma Physics.

FIGURE CAPTIONS

Fig. 1 : The frequency spectrum is shown for a currentless plasma slab with uniform density as a function of axial wavenumber k, for (a) m = ± 1 and (b) m = ± 2. The first and second radial modes are designated by $F_1^{\pm}$ and $F_2^{\pm}$ accordingly to whether m > 0 or m < 0. The notation "S" stands for "surface mode", which coincides with F_1^-. The dot-dashed line (-.-) represents the accumulation point forthe frequencies of the Alfvén wave, with $\omega_{ci} = 2$.

Fig. 2 : The position of optimal resonance layer (a) and optimal power (b) is plotted as a function of the axial wavenumber k for m = +1. Curve (1) refers to standard MHD conditions; whereas, curve (2) refers to the currentless, i.e., shearless case. The gravity field is zero in both cases.

Fig. 3 : The absorbed power is plotted as a function of the position x_R of the resonant surface for (1) k = 0.01, (2) k = 1.01 and (3) k = 2.01. In all cases, m = +1. The results shown are for MHD standard conditions (a) without and (b) with gravity. The scanning step used for x_R is, Δx_R = 0.05.

Fig. 4 : The absorbed power is plotted as a function of the position, x_R, of the resonant surface for ω/ω_{ci} = 0.0, 0.2, 0.4, 0.6 (curves labelled 1, 2, 3, 4). In all cases gravity was not included and m = + 1. In (a) k = 0.2, and in (b) k = 0.5. In both cases $\Delta x_R = 0.05$.

Fig. 5 : The absorbed power is plotted as a function of the position of the resonant surface for ω/ω_{ci} = 0.0, 0.2, 0.4, 0.6 (curves labelled 1, 2, 3, 4). In (a), k = -1.5, m = -1 and in (b), k = +1.5, m = +1. Standard conditions without gravity are used, and Δx_R = 0.05.

Fig. 6 : The global modes of the Alfvén wave for m = +1 are shown. Standard MHD conditions with consistent gravity are used for curve (1). Artificial step-wise gravity with g = 0.35, 0.70, 1.0 is used for curves (2, 3, 4). The marked line represents the lower edge of the Alfvén continuum.

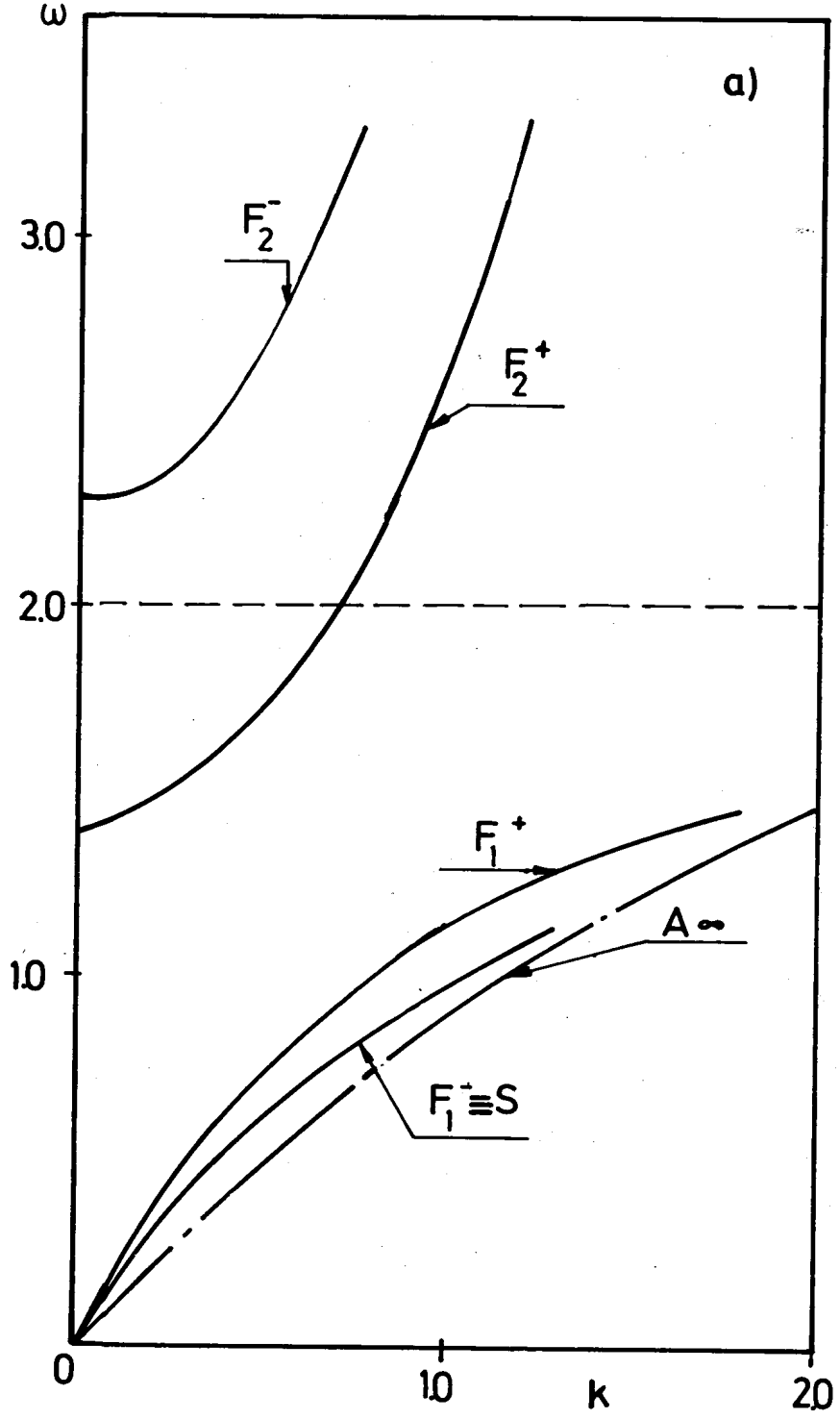
ω
a)
3.0
2.0
1.0
0
1.0
k
2.0
F_2^-
F_2^+
F_1^+
A_∞
$F_1^-\equiv S$

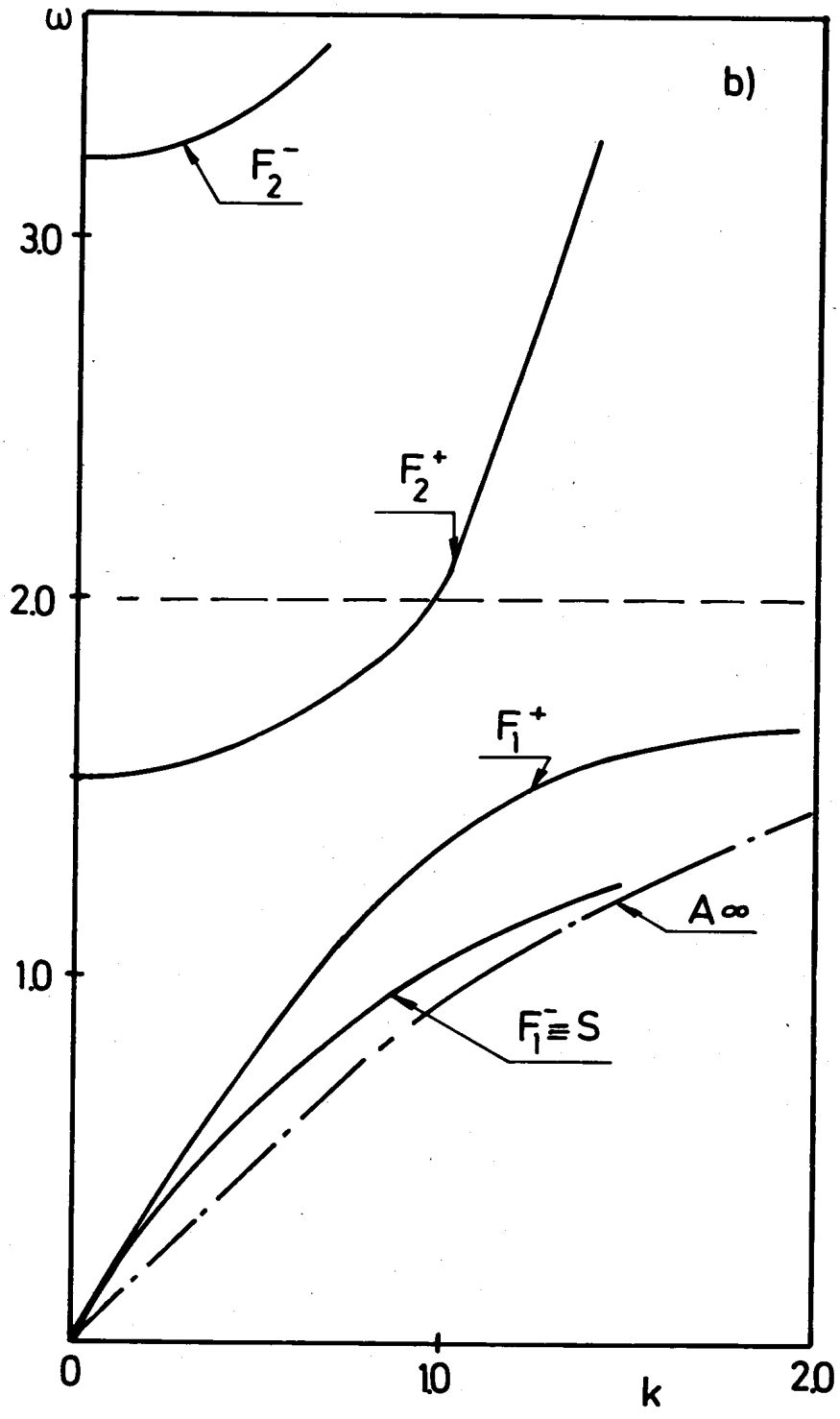
ω
b)
3.0
2.0
1.0
0
1.0
k
2.0
F_2^-
F_2^+
F_1^+
A_∞
$F_1^-\equiv S$

FIG. 1

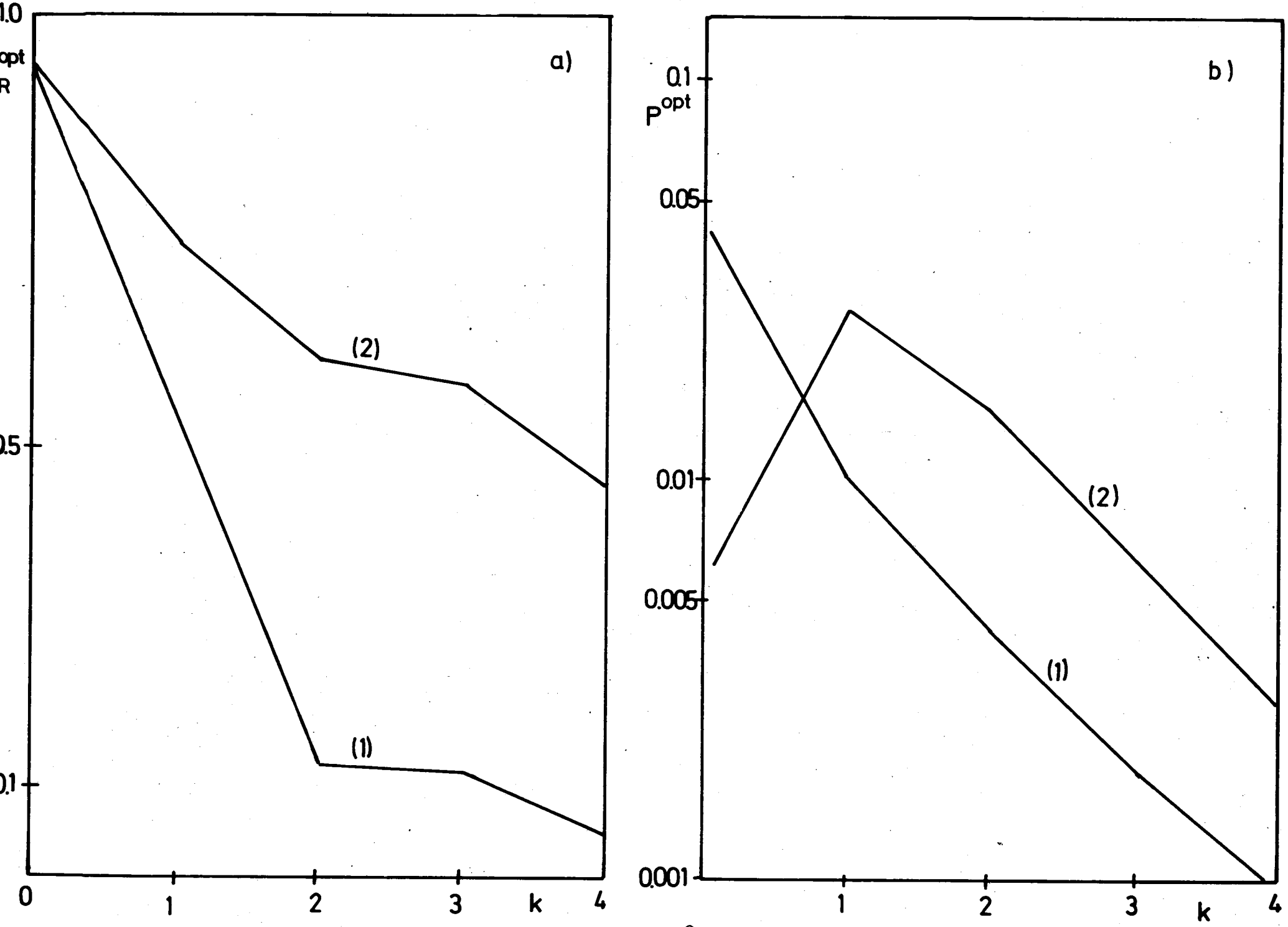

FIG. 2

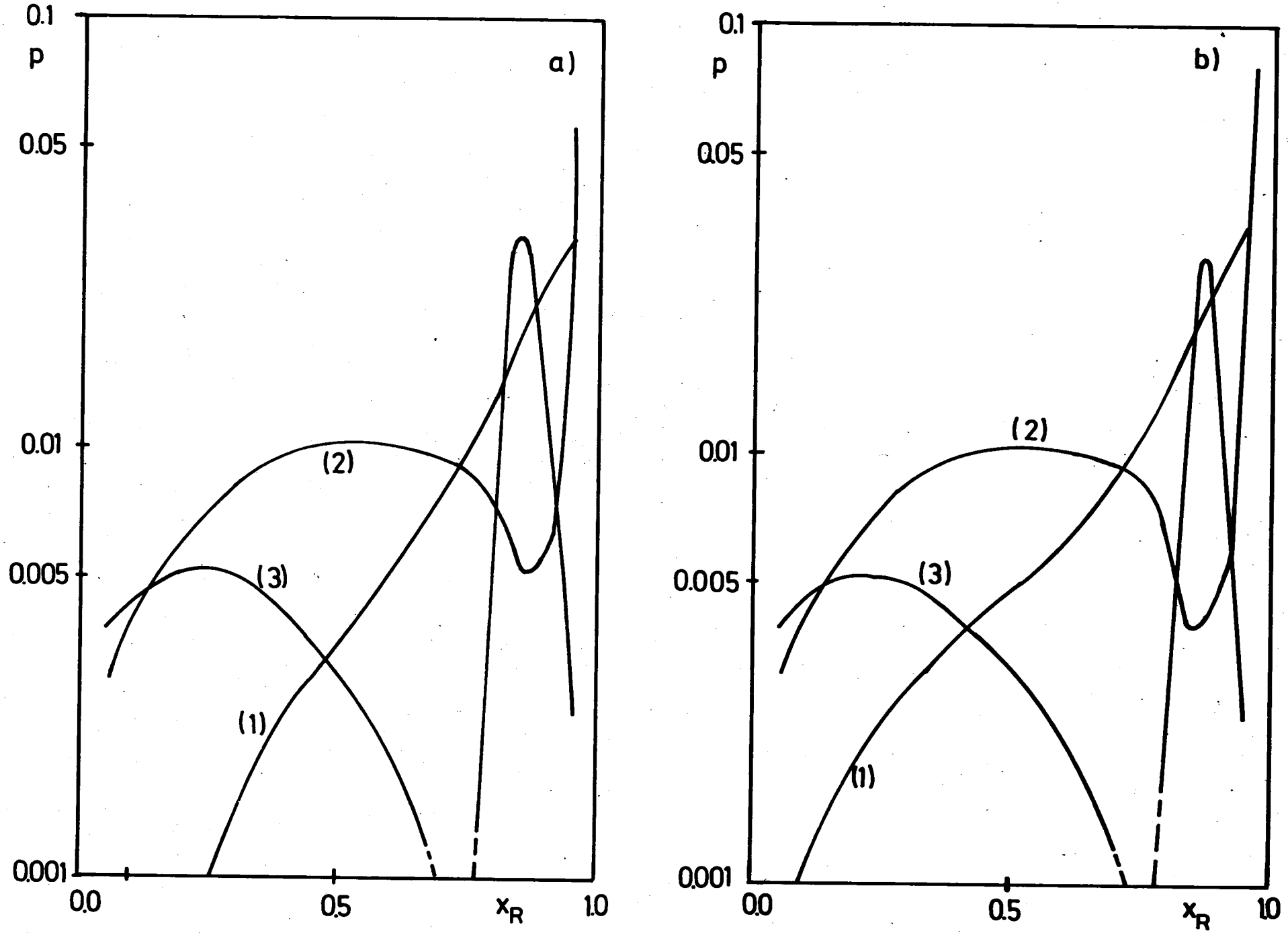
0.1
p
a)
0.05
0.01
0.005
0.001
(2)
(3)
(1)
0.0
0.5
x_R
1.0
0.1
p
b)
0.05
0.01
0.005
0.001
(2)
(3)
(1)
0.0
0.5
x_R
1.0

FIG. 3

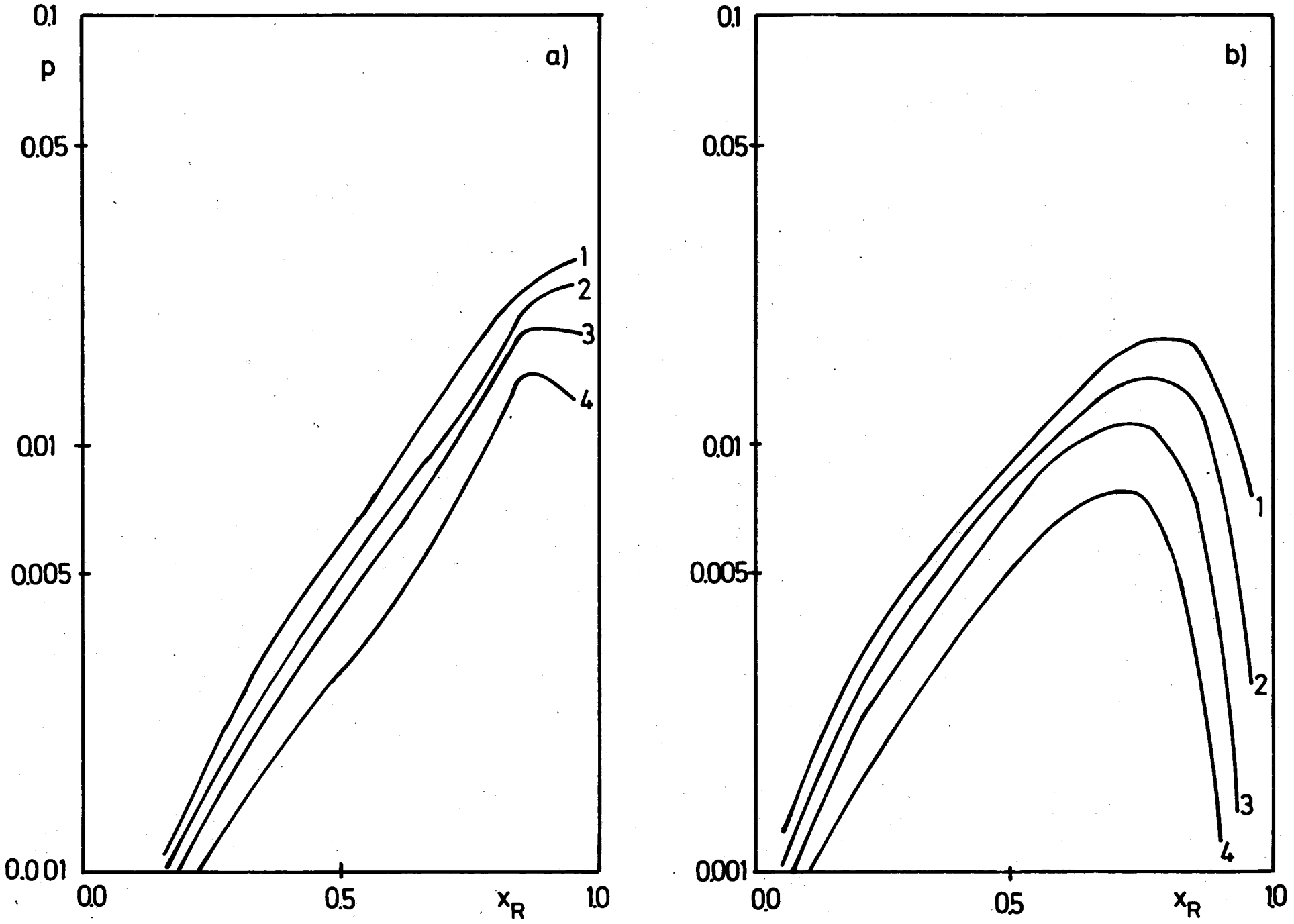
0.1
p
0.05
0.01
0.005
0.0 01
a)
1
2
3
4
0.0
0.5
x_R
1.0
0.1
0.05
0.01
0.005
0.001
b)
1
2
3
4
0.0
0.5
x_R
1.0

FIG. 4

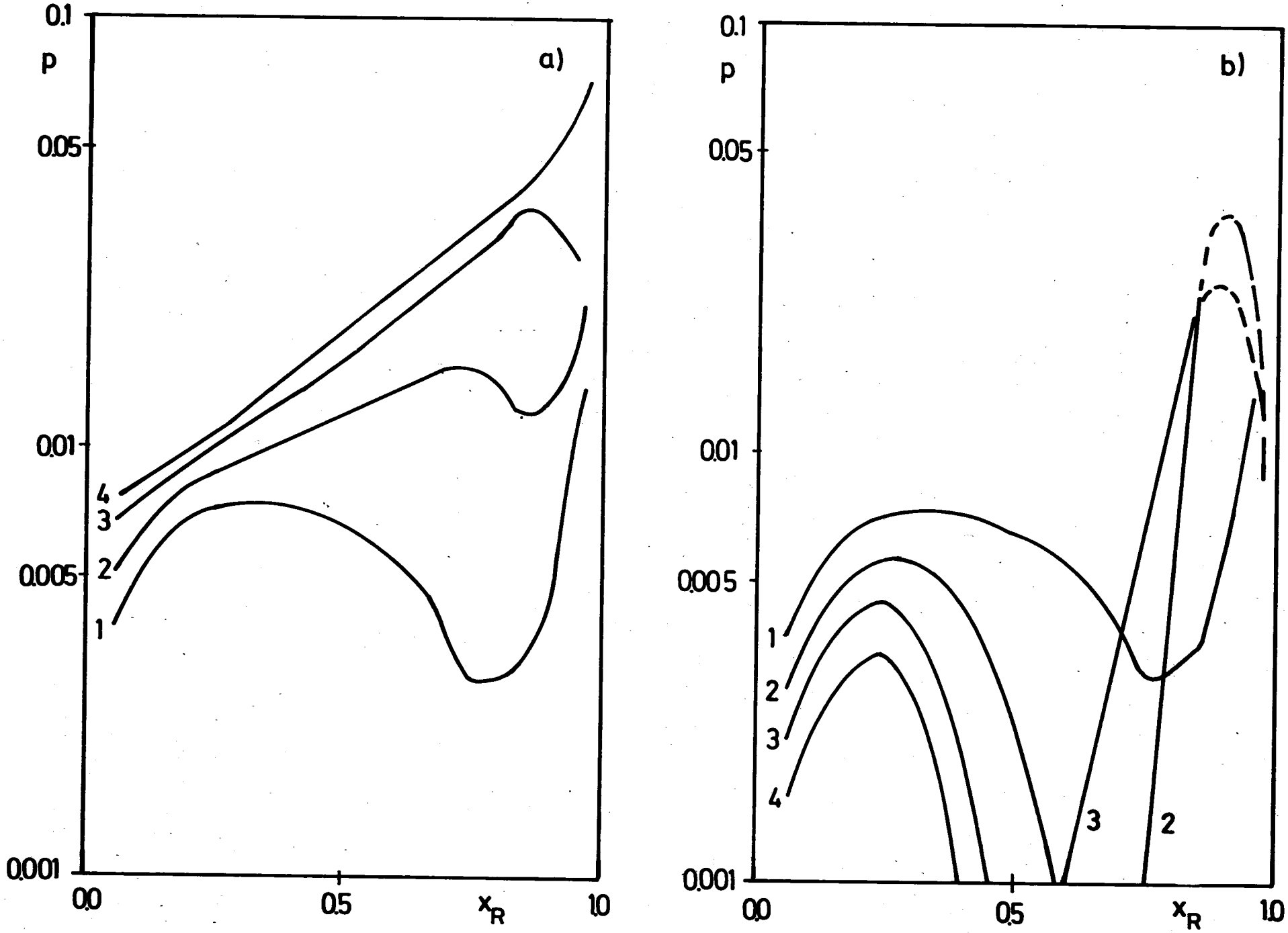

FIG. 5

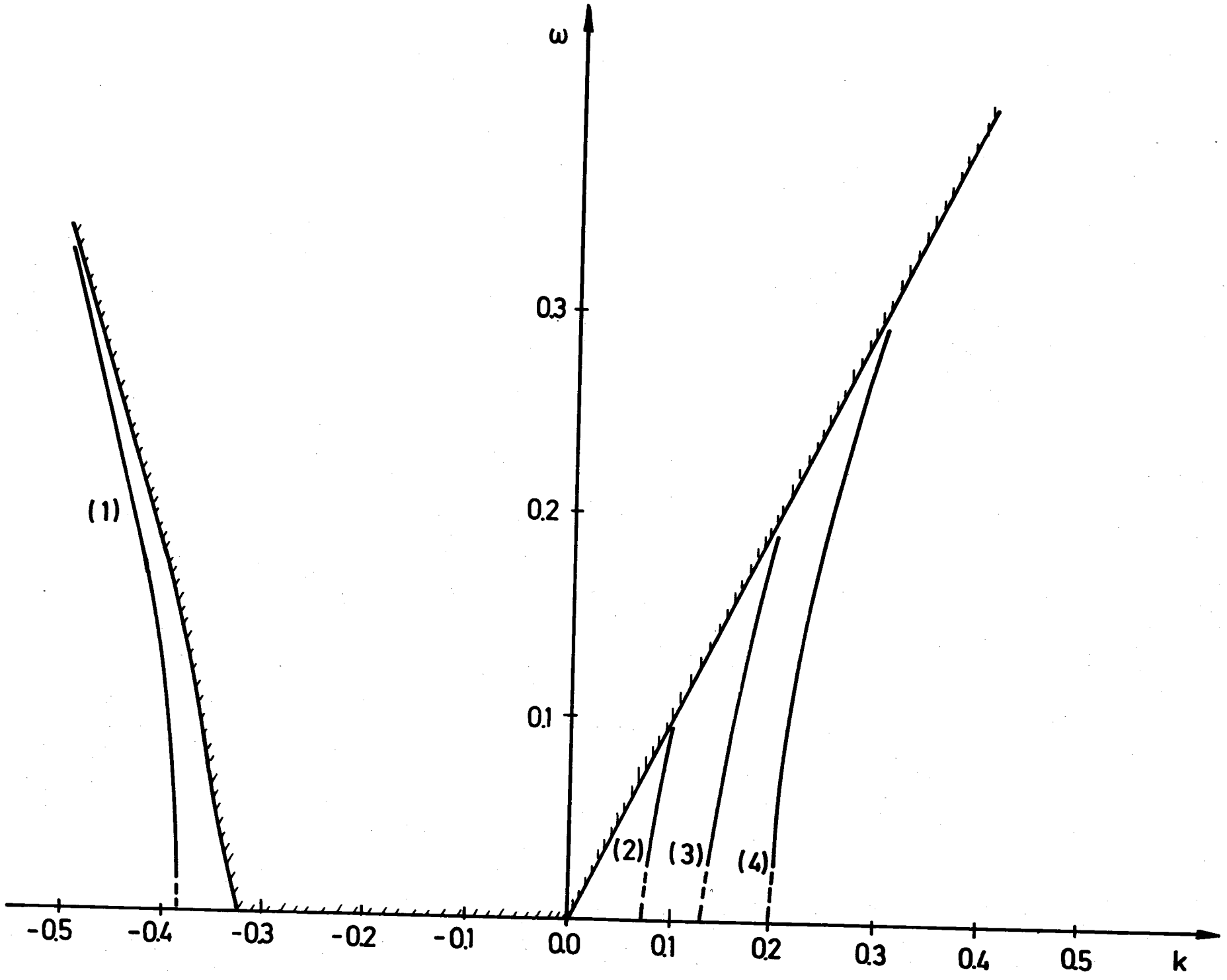

FIG. 6